

SUPPORTING INFORMATION

Observation of two-step spin transition in iron(II) 4-amino-1,2,4-triazole based spin crossover nanoparticles.

Nikolia Lalioti,^{*a} Efstathia Giannopoulou,^a Alexander Charitos,^a John Parthenios,^b Ondrej Malina,^{*c} Michaela Polaskova,^c Alexandros Kalarakis,^d Vassilis Tangoulis^{*a}

^a Department of Chemistry, Laboratory of Inorganic Chemistry, University of Patras, 26504 Patras, Greece. Email: lali@upatras.gr; vtango@upatras.gr

^bInstitute of Chemical Engineering Sciences, Foundation of Research and Technology-Hellas (FORTH/ICE-HT), Stadiou Street, Platani, Patras, 26504 Greece

^cRegional Centre of Advanced Technologies and Materials, Czech Advanced Technology and Research Institute (CATRIN), Palacký University Olomouc, Křížkovského 511/8, 77900, Czech Republic. Email: ondrej.malina@upol.cz

^dDepartment of Mechanical Engineering, University of the Peloponnese, 26334 Patras, Greece

EXPERIMENTAL SECTION

Materials and Methods

All manipulations were performed under aerobic conditions using reagents and solvents (Alfa Aesar, Sigma Aldrich, Serva) as received. The ligand 4-amino-4H-1,2,4-triazole (NH_2trz), was purchased from Alfa-Aesar, iron(II)bromide hexahydrate salt, $\text{FeBr}_2 \cdot 6\text{H}_2\text{O}$ and *n*-hexanol from Sigma Aldrich. Triton X-100 and cyclohexane were obtained from Serva. Graphene oxide, dry powder, GO, was procured from Abalonyx, Norway, product 18002: <100 mesh. The deionized water used for synthesis was deoxygenated by simultaneous sonication and argon bubbling for 1 h.

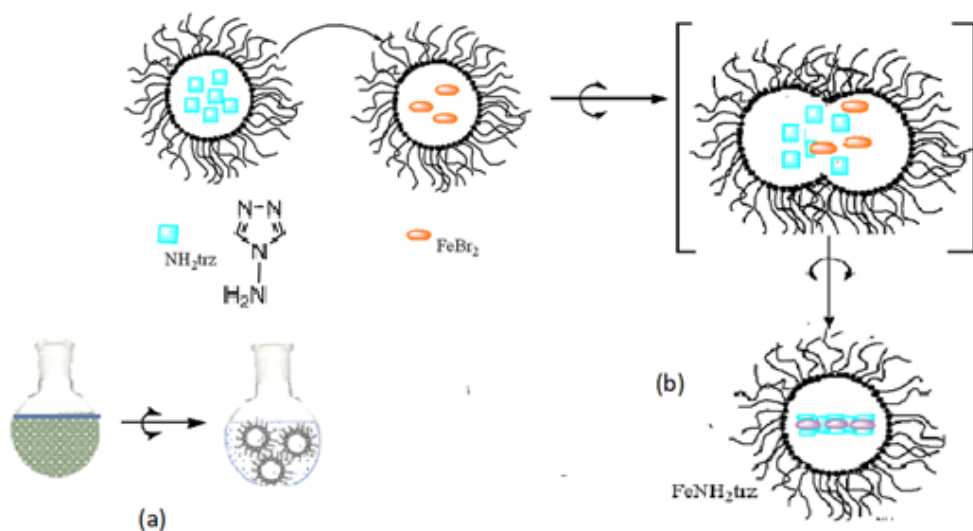
Synthesis of nanoparticles NP1-3

[Fe(NH_2trz) $_3$](Br) $_2$ ·3H $_2$ O·0.02 TX100 NP1. An aqueous solution of $\text{FeBr}_2 \cdot 6\text{H}_2\text{O}$ (216 mg, 1 mmol in 0.5 mL of deionized H $_2$ O) and 5 mg of ascorbic acid added to a solution containing Triton X-100 (1.8 mL), *n*-hexanol (1.8 mL) and cyclohexane (7.5 mL). The resulting mixture was stirred until the formation of a clear water-in-oil microemulsion. A similar procedure was applied to 1,2,4-1 amino-triazole (NH_2trz) (252 mg, 3 mmol in 0.5 mL of deionized H $_2$ O). The ligand microemulsion was added to the metal microemulsion and the mixture was stirred for 20h. The colour changed right after the addition of acetone (15 mL) from white to pink. The addition of acetone destabilizes the final microemulsion and promotes the precipitation of the NPs. The nanoparticles were extracted by centrifugation, washed with EtOH (3x12mL) and AcO (1x12mL) for the removal of the surfactant and finally dried under vacuum (0.1 mbar, 24 h). Yield: 332 mg (0,62 mmol, 62%).

[Fe(NH_2trz) $_3$](Br) $_2$ ·3H $_2$ O·0.04 TX100, NP2. The material was prepared following the same synthetic procedure as in sample NP1 but using triton X-100 (4,2 ml), *n*-hexanol (1.8 mL), and cyclohexane (5.1 mL). Yield: 265mg (0,45 mmol/45%)

[Fe(NH_2trz) $_3$](Br) $_2$ ·3H $_2$ O·0.02 TX100, NP3. The material was prepared following the same synthetic procedure as in sample 1 but stirred for 48h instead of 20h. Yield: 427 mg (0,80 mmol, 80%).

Nanoparticles of the SCO polymer $[\text{Fe}(\text{NH}_2\text{trz})_3\text{Br}_2 \cdot 3\text{H}_2\text{O}$ **1–3** were prepared by the reverse micelle method at ambient conditions. The synthetic pathway is present in Scheme 1. Two separate aqueous solutions were initially prepared in ambient conditions. An aqueous solution of iron(II) salt with a small amount of ascorbic acid and an aqueous solution containing the stoichiometric amount of the ligand (NH_2trz). Each of these was mixed with a previously prepared solution of Triton X-100 (surfactant), *n*-hexanol (co-surfactant) and cyclohexane (solvent). To prepare stable microemulsions the two mixtures were shaken with a vortex system (2 min) and vigorously stirred for 30 min. The two microemulsions were mixed, adding the ligand to the metal, and stirred for several hours to allow the micellar exchange. The above procedure was repeated several times to confirm the reproducibility of NPs synthesis. Variants of the synthetic parameters were also studied such as i) modification of the ω_0 parameter i.e., changing the amounts of Triton X-100 and *n*-hexanol keeping constant the water amount and ii) increasing the reaction time from 20 to 48 h.



Scheme 1. Schematic representation of the (a) formation of a clear water-in-oil microemulsion and (b) the reverse micelles synthetic method of the FeNH_2trz NPs.

PHYSICAL MEASUREMENTS

Elemental analyses (C, H, N) were performed by the in-house facilities of the University of Patras (Greece). IR spectra (4000-400 cm^{-1}) were recorded using a Perkin-Elmer 16PC FT-IR spectrometer with samples prepared as KBr pellets.

Raman measurements were carried out using a Renishaw in Via Raman spectrometer in the backscattering geometry. The beam of a solid-state 515 nm (Cobalt Fandango) laser was focused by means of a 50 \times objective lens (NA 0.75) yielding a laser spot size of about 1 μm . The Raman scattered radiation was dispersed by a 2400 grooves mm^{-1} diffraction grating. For ease of comparison, most measurements of all samples resulted after 5 accumulations with laser powers of 85 and 340 μW respectively with an exposure time of 30s each. After acquiring the common protocol spectra as explained above, the thermal tolerance of each sample was examined. Increased laser power and exposure time eventually resulted in the formation of Iron Oxide, which was then confirmed by a Raman measurement with the laser beam focused on the visibly damaged area of the sample.

The powder X-ray diffraction (p-XRD) measurements were performed at room temperature on a Bruker D8 Advance diffractometer with focusing $\text{K}\alpha 1$ geometry. Polycrystalline samples were loaded in 1 mm borosilicate glass capillaries while the X-ray tube operated at 45 kV and 40 mA. The incident-beam side ($\text{CuK}\alpha 1$ radiation, $\lambda = 1.54056 \text{ \AA}$) is equipped with a focusing X-ray mirror, a 0.5 $^\circ$ fixed divergence slit, 0.5 $^\circ$ anti-scatter slits and 0.04 rad Soller slits, while on the diffracted-beam side the system was configured with 0.04 rad Soller slits and a PIXcel1D detector with anti-scatter shielding. Four scans were performed in Debye-Scherrer mode, with a step size of 0.0066 $^\circ$ on a spinning stage ($\sim 300 \text{ rpm}$), within a 2θ range of 4.0–90.0 $^\circ$. No radiation damage was observed even after 5 h of measurement, therefore all scans were merged to increase counting statistics. The broadening of the Bragg peaks also due to instrumental reasons (β_{inst}) has been deduced from the observed integral breadth (bobs) considering the instrumental contribution is mainly of the Gaussian form, $\beta_{mat}^2 = \beta_{obs}^2 - \beta_{inst}^2$. The value of β_{inst} was determined by using a well characterised LaB_6 powder sample in which the crystallite sizes are $>1000 \text{ nm}$, such as the broadening of the Bragg peaks only originates from the instrument. The parameter β_{inst} is a function of the Bragg angle, but not in the small angle region used in this study ($2\theta < 20^\circ$) at which it is constant and equal to 0.1108.

TEM study was performed utilizing an FEI CM20 TEM operating at 200 kV. TEM specimens were prepared by drop-casting a 3 μL droplet of nanoparticles suspension in

acetone on a carbon-coated Cu TEM grid. The size of the particles is determined by “manual counting” using ImageJ software (<https://imagej.net>).

The direct-current (DC) magnetic susceptibility measurements were measured on powder samples using a physical-properties measurement system (PPMS, Quantum Design) at 200-400-200 K thermal loops with a rate of 1.0 K min⁻¹ under an applied dc magnetic field of 1000 Oe. The experimental data were corrected for the diamagnetism and signal of the sample holder and the Pascal constants were used for the diamagnetic corrections.

Differential Scanning Calorimetry (DSC) measurements were carried out in an N-(g) atmosphere using a DSC (Q100, TA Instruments, USA) instrument. Pin-hole aluminum hermetic pans were used to encapsulate 5-7 mg of the sample. The pans were purged with nitrogen at a rate of 50 mL min⁻¹ and liquid nitrogen was used for cooling. Initially, the samples were cooled down from 253 K to 410 K at a rate of 10 K/min. Then the samples were subjected to three successive thermal regimes; (a) heating from 253 K to 410 K at a rate of 10 K min⁻¹ and (b) cooling to 253 K at the same rate. At the beginning and end of each heating and cooling run the sample was held isothermally for 5 min.

Thermogravimetric Analysis (TGA) was performed using SETA-RAM SetSys-1200 and carried out at a heating rate of 1 °C min⁻¹ under a N₂ atmosphere.

DLS measurements were performed using a ZetaSizer Zen3600 (Malvern Instruments). The sample was loaded into a disposable micro cuvette and measured at 25 °C. The intensity size distribution or the Z-average diameter was obtained using the cumulant analysis with a repeatability of 1.6%.

Elemental Analyses

Table S1. Elemental analyses for NP1 - 3

Sample NP		C [%]	N [%]	H [%]	Molecular Formulae
1	exptl	14.88	31.50	3.61	Fe(NH₂trz)₃]Br₂·3H₂O 0.02TX100
	calcd	14.97	31.46	3.48	534.36 g/mol
2	exptl	15.89	30.88	3.84	Fe(NH₂trz)₃]Br₂·3H₂O 0.04TX100
	calcd	16.08	30.73	3.78	546.94 g/mol
3	exptl	14.82	31.53	3.39	Fe(NH₂trz)₃]Br₂·3H₂O 0.02TX100
	calcd	14.97	31.46	3.48	534.36 g/mol

TEM Study

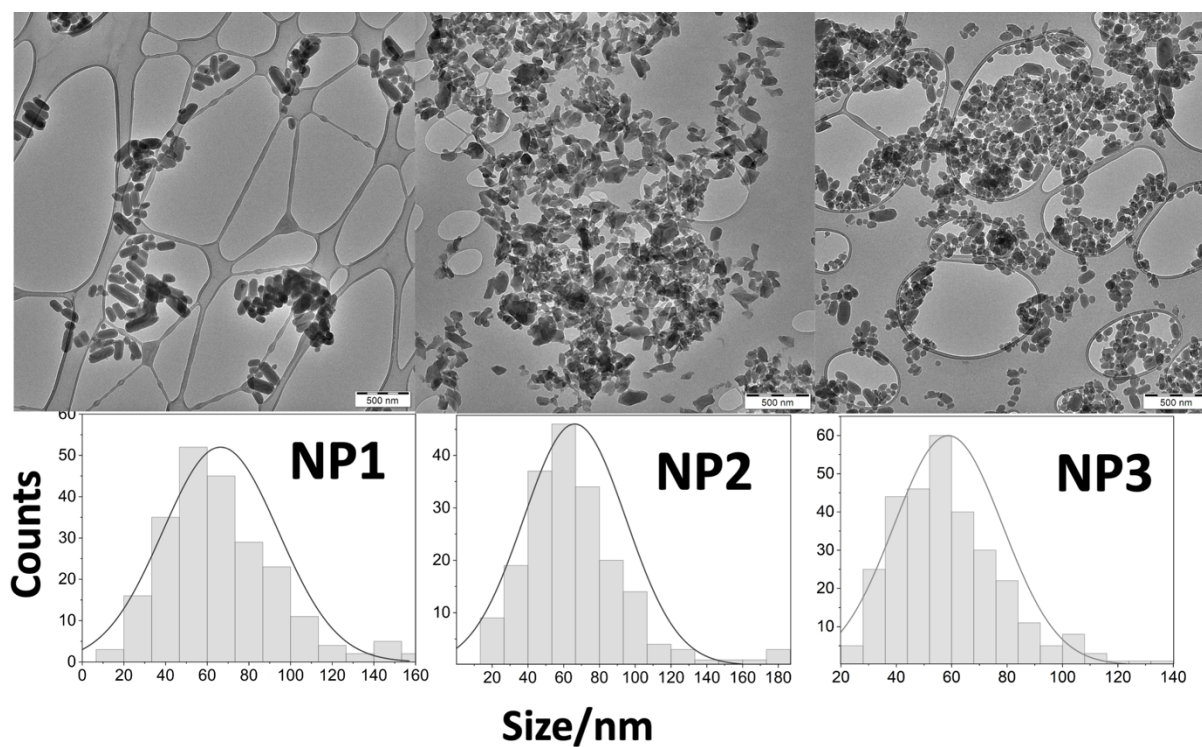


Figure S1. TEM images of **NP1-3** with Gaussian distributions of sizes.

Table S2. Average distribution sizes of the studied SCO NPs derived from TEM measurements, calculated average apparent domain size, $\langle L_V \rangle$, and diameter if the coherent domains, $\langle D \rangle$, from pXRD measurements and the average number of domains per nanoparticle, $\langle N_D \rangle$.

NPs	Distribution size [nm]	$\langle L_V \rangle$ [nm]	$\langle D \rangle$ [nm]	$\langle N_D \rangle$
NP1	70	10	13	160
NP2	70	8	10	350
NP3	60	18	24	16

IR Spectra

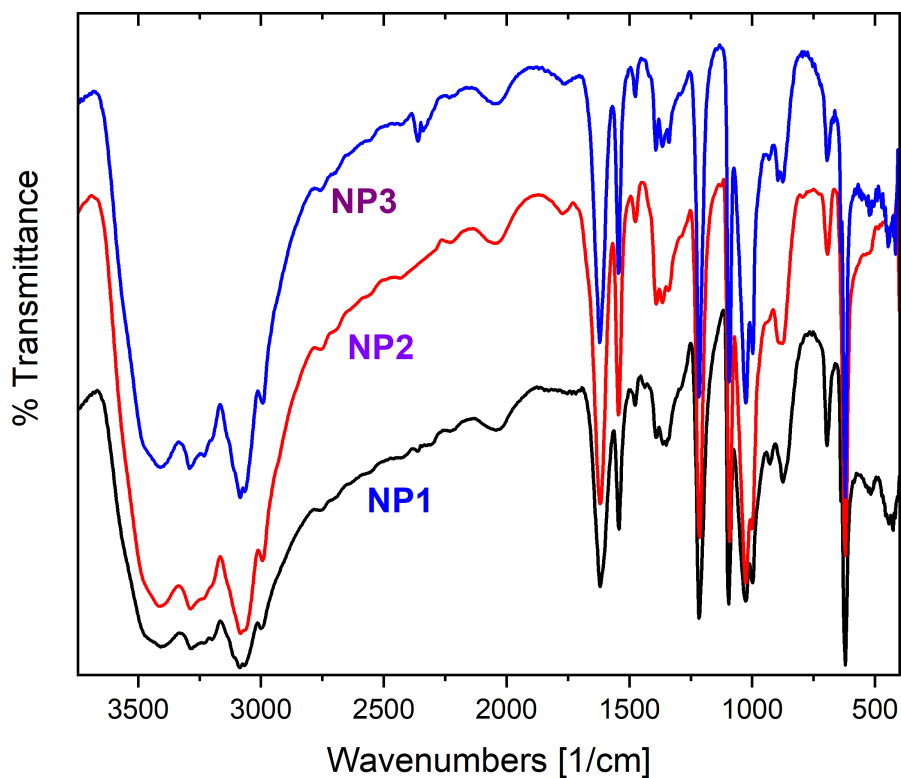


Figure S2. IR spectra of the NP1 – 3.

Table S3. Assignment of the observed bands in the IR spectra of the NP1 – 3.

$[\text{Fe}(\text{atrz})_3](\text{Br})_2$	description,	$[\text{Fe}(\text{atrz})_3](\text{Br})_2$	description,
3410s-3285 s, br	$\nu(\text{NH}_2)$ $\nu(\text{NH}_2)$ $\nu(\text{OH})$ water	1093s	$\delta(\text{CH})$
3085s	$\nu(\text{CH})$ stretch	1026s	R_6 ring stretch
1620s	$\delta(\text{NH}_2)$	1000m	R_7 ring breathing
1545s	R_1 ring stretch	891m, br	$\gamma(\text{CH})$ bend
1475m	R_2 ring stretch	876m	$\beta(\text{NH}_2)$
1390m, br	R_3 ring stretch	693m	R_8 ring torsion
1215s	$\nu(\text{N-NH}_2)$	621s	R_9 ring torsion

m = medium, w = weak, br = broad, and s = strong

TGA measurements

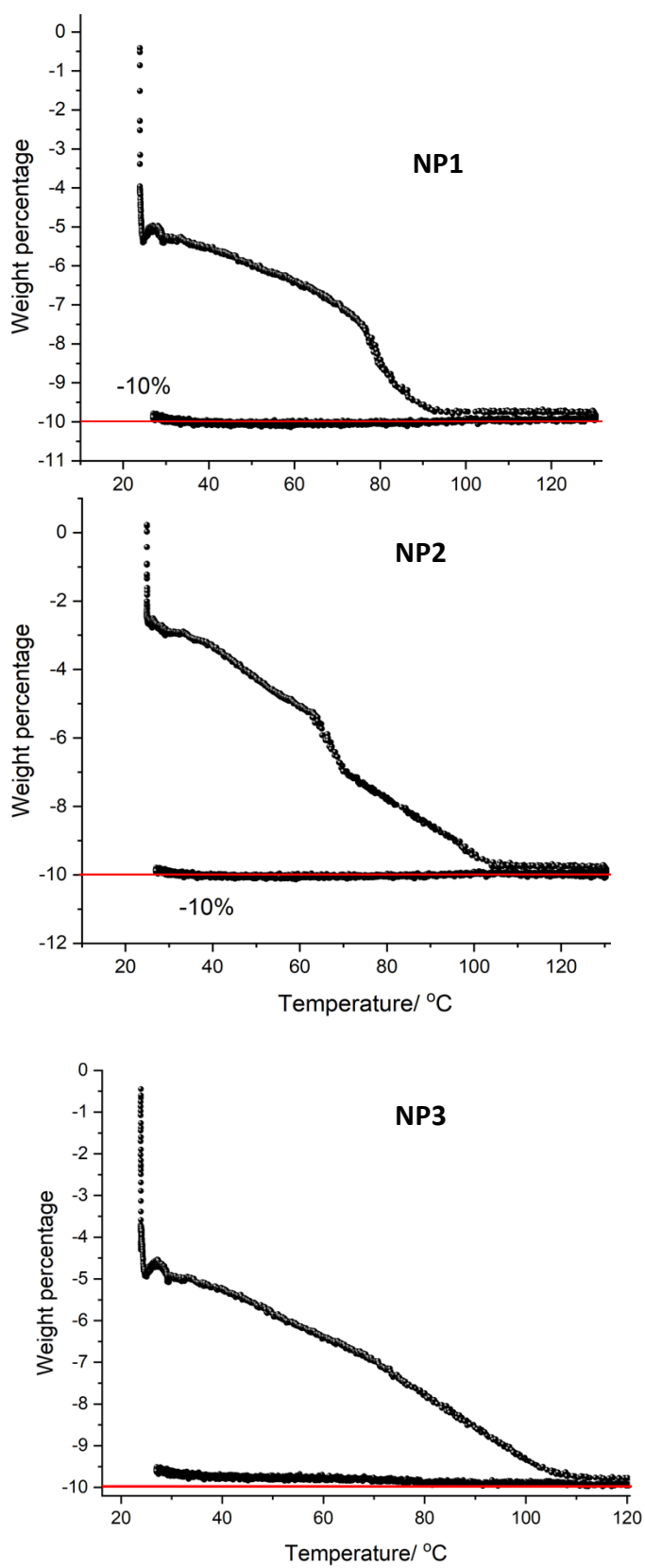


Figure S3. Thermogravimetric measurements of NP1-3.

DLS measurements

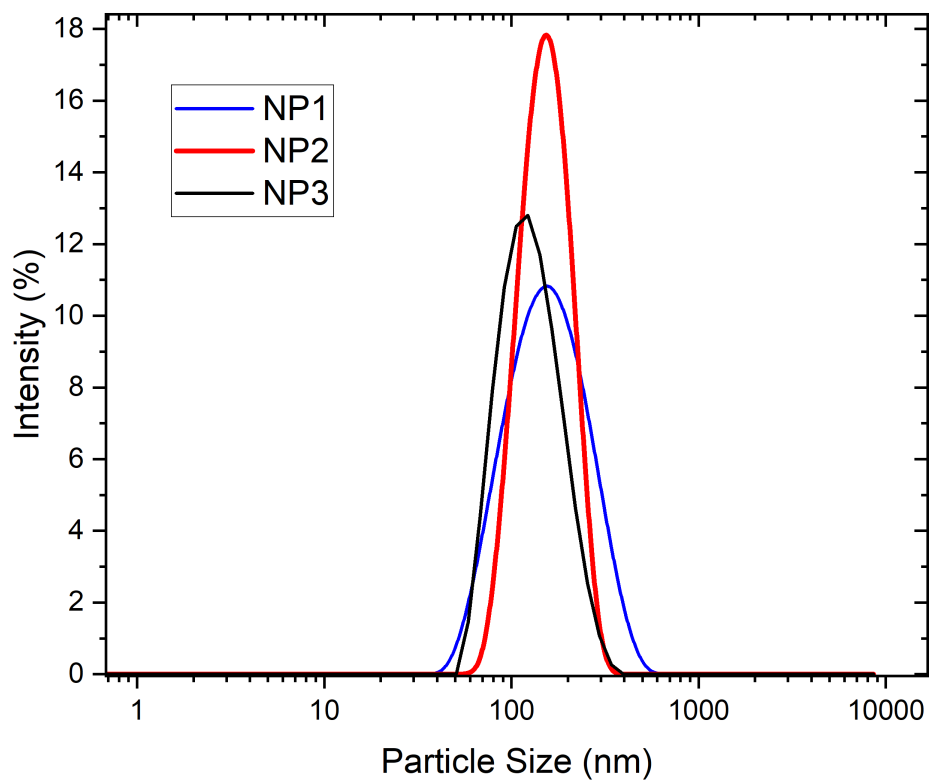


Figure S4. DLS measurements of NP1-3.

Magnetic Measurements

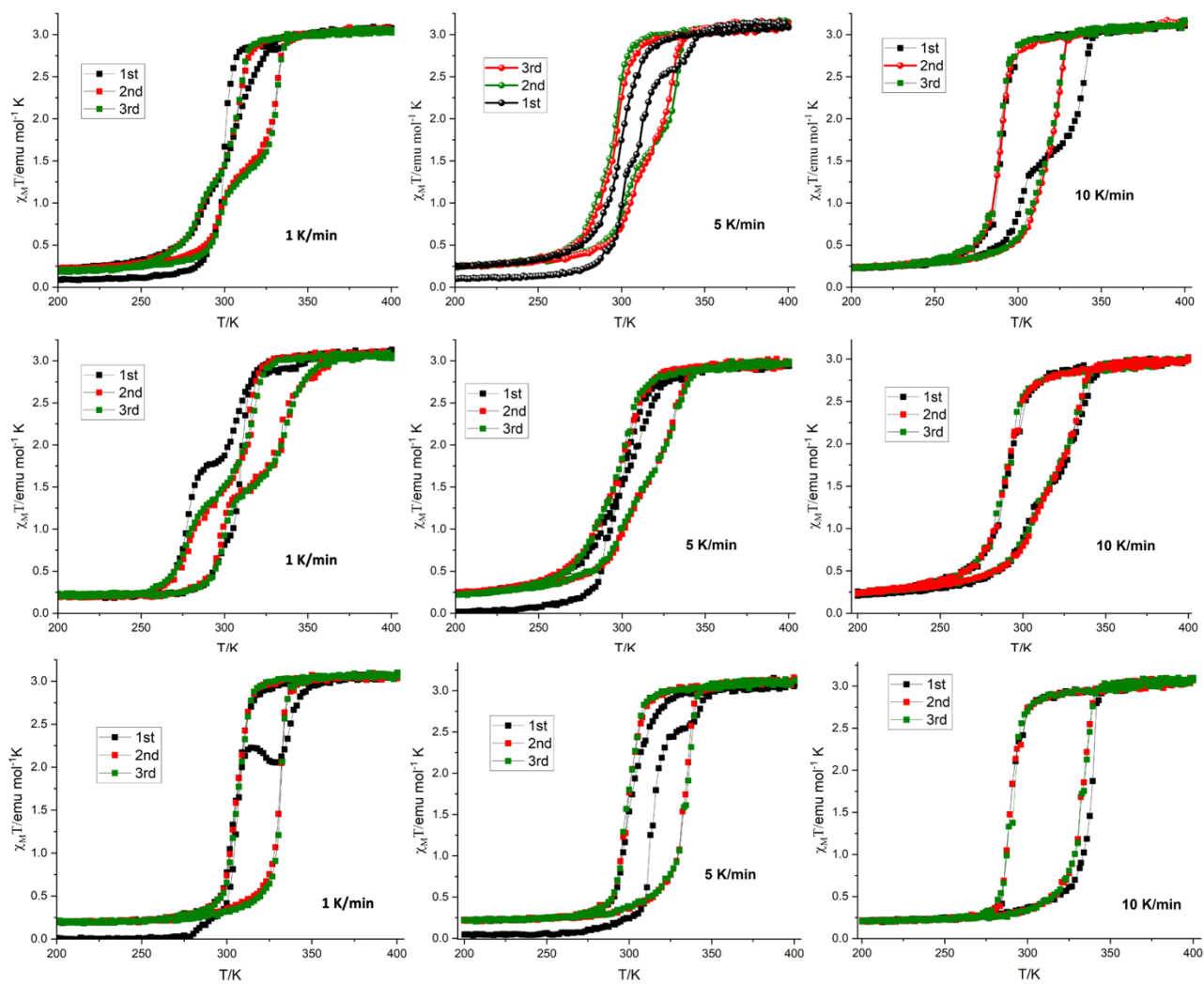


Figure S5. Thermal loops (3 cycles) at different magnetic sweep rates 1K/min, 5 K/min and 10 K/min; (first row) NP1; (second row) NP2; (third row) NP3.

DSC Measurements

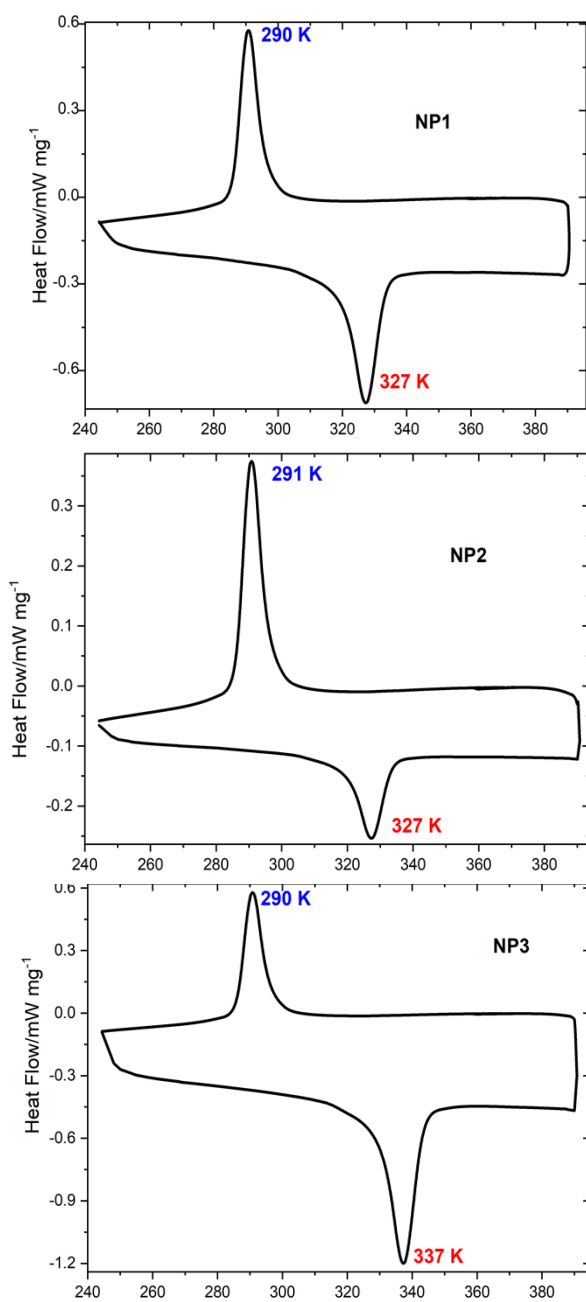


Figure S6. DSC curves of **NP1-3** presenting the 3rd heating-cooling cycle at 10 K/min.

Table S4. General synthetic protocol, critical temperatures derived from the DSC measurements and from the thermal magnetic hysteresis for the studied SCO NPs.

NPs	ω	t	DSC			MAGNETIC		
			T _{up} (K)	T _{down} (K)	ΔT (K)	T _{up} (K)	T _{down} (K)	ΔT (K)
NP1	10	20 h				1 K/min		
						296	283	13
						332	309	22
						5 K/min		
						306	295	
						330		
			10 K/min					
			327	290	37	326	292	34
NP2	4	20 h				1 K/min		
						296	278	18
						336	318	18
						5 K/min		
						304	298	
						327		
			10 K/min					
			327	291	36	328	292	36
NP3	10	2 d				1 K/min		
						333	306	27
						5 K/min		
						335	300	35
						10 K/min		
						337	290	47

RAMAN STUDY

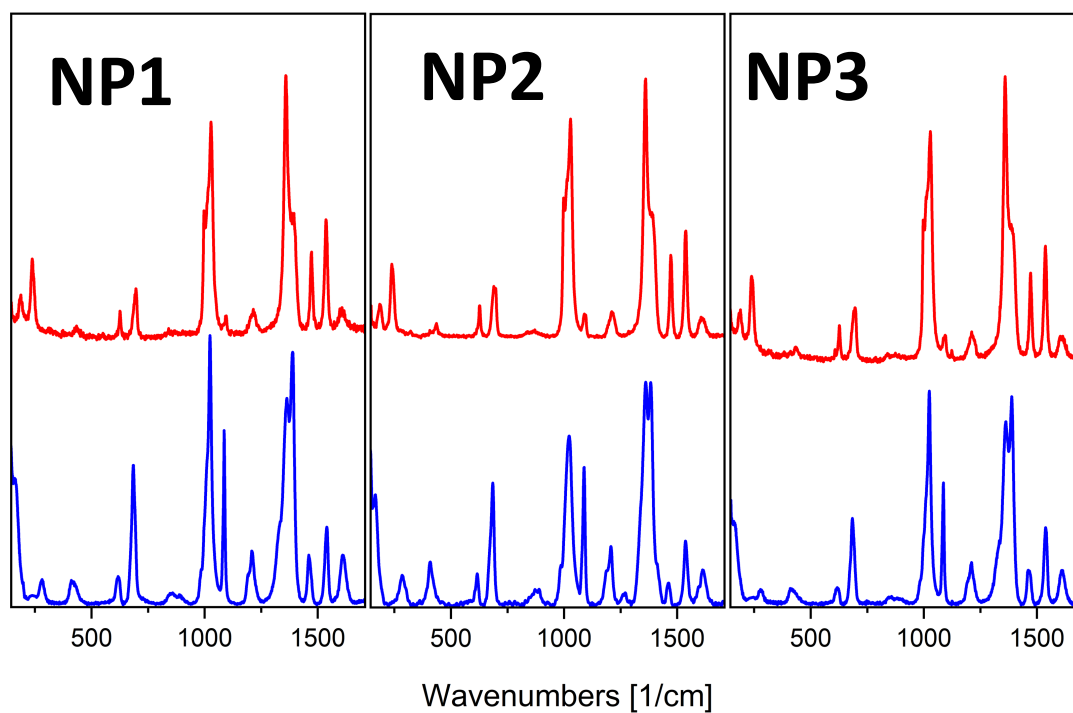


Figure S7. Comparison of HS/LS spectra of NPs 1-3 in the range of 150-1700 cm^{-1}

Table S5. Peak assignments of [Fe(NH₂trz)₃]Br₂ nanoparticles (NPs **1-5**) in the diamagnetic low spin state(s=0). Meaning of symbols: L, librations; T, translations; ν : stretching; δ : deformation or in-plane bending; ω , wagging; τ : torsion; rg : ring)

Appx. wavenumber region (cm ⁻¹)	Peak assignment	Vibrational mode
195	NH ₂ -trz	L
248	NH ₂ -tz	T
445	C-N-NH ₂	δ
635	NH ₂	ω
702	N-NH ₂	ν , τrg
1006	N-N	ν
1037	N-N	δrg
1104	C-NNH ₂ , H-C-N	δrg , ν , δ
1218	H-C-N	δ
1368	C-NNH ₂	ν
1398	C-N, N-NH ₂	ν , ν
1478	C-N	ν
1545	C-N, C-NNH ₂ , H-C-N	ν , ν , δ
1616	NH ₂	δ